

Structural Integrity of Functionally Graded Composite Structure using Mindlin-type Element

O.O. Oyekoya, D.U. Mba¹ and A.M. El-Zafrany

Abstract: In this paper, two new Mindlin-type plate bending elements have been derived for the modelling of functionally graded plate subjected to various loading conditions such as tensile loading, in-plane bending and out-of-plane bending. The properties of the first Mindlin-type element (i.e. Average Mindlin-type element) are computed by using an average fibre distribution technique which averages the macro-mechanical properties over each element. The properties of the second Mindlin-type element (i.e. Smooth Mindlin-type element) are computed by using a smooth fibre distribution technique, which directly uses the macro-mechanical properties at Gaussian quadrature points of each element. There were two types of non-linearity considered in the modelling of the plate, which include finite strain and material degradation. The composite plate considered in this paper is functionally graded in the longitudinal direction only, but the FE code developed is capable of analysing composite plates with functional gradation in transverse and radial direction as well. This study was able to show that the structural integrity enhancement and strength maximisation of composite structures are achievable through functional gradation of material properties over the structure.

Keyword: Functionally graded material, finite element methods, Mindlin-type plate bending theory, finite strain, progressive damage analysis.

List of Symbols

B	Matrix of shape function derivatives
F	Nodal load vector
K	Element stiffness matrix
R	Residual vector
γ	Transverse shear strain vector
σ	x-y stress vector
τ	Transverse shear stress vector

¹ School of Engineering, Cranfield University, Cranfield, Bedfordshire, MK43 0AL, England.

$\boldsymbol{\epsilon}$	x-y strain vector
U	Strain energy
u, v, w	Displacements
V	Volume fraction
W	Work done by actual load
X	Longitudinal strength
Y	Transverse strength
μ	Shear modulus
ν	Poisson ratio
$()_1$	Longitudinal direction of the material axis
$()_2$	Transverse direction of the material axis
$()_c$	Compressive strength
$()_f$	Fibre
$()_m$	Matrix
$()_t$	Tensile strength
$()_x$	Longitudinal direction of the local axis
$()_y$	Transverse direction of the local axis
$()_{comp}$	Traditional composite
$()_{fgm}$	Functionally graded material
$()^L$	L^{th} layer of composite
$()^o$	Midplane of composite
$()^\sigma$	Non-linear terms

1 Introduction

Composite materials are often used in different engineering fields, especially in the aerospace field. The advantage of composite materials is the high stiffness-to-weight and strength-to-weight ratios. The limitations of composite materials are the following: the weakness of interfaces between layers may lead to de-lamination, extreme thermal loads may lead to de-bonding between matrix and fibre due to mismatch of mechanical properties, and residual stresses may be present due to difference in coefficients of thermal expansion of the fibre and the matrix. To overcome the limitations, functionally graded materials (FGMs) were proposed. The FGMs are made in such a way that the volume fractions of two or more materials are varied continuously along a certain dimension. The FGMs can be made as required for different applications. For example, thermal barrier plate structures can be made from a mixture of ceramic and metal for high temperature application. The advantage of the FGM plate is that its material properties vary continuously from one surface to the other, hence avoiding the interface problem that exists in homogeneous composites. The FGM concept originated in Japan in 1984 during

the space-plane project, in the form of a proposed thermal barrier material capable of withstanding a surface temperature of 2000 K and a temperature gradient of 1000 K across a cross section <10 mm.

In the modelling and simulation of FGMs, many researchers have implemented different numerical techniques. These include boundary element method (BEM) [Criado et. al. (2007), Chen and Liew (2004)], meshless local Petrov-Galerkin (MLPG) method [Wen et. al. (2008), Liu et. al. (2008), Sladek et. al. (2008), Ching and Chen (2006)] and finite element method (FEM) [Reddy (2000)].

Chen and Liew (2004) investigated the buckling behaviour of FGM rectangular plates subjected to non-linearly distributed in-plane edge loads. They stated that a mesh-free method which approximates displacements based on scattered nodes (i.e. radial basis function and polynomial basis) was employed, in-order to avoid complicated numerical procedures that arises in the FEM from the use of elements. This FEM complication was dealt with in this paper. Reddy (2000) presented a theoretical formulation and finite element models based on third order shear deformation theory for the analysis of through-thickness functionally graded plates. The Navier solution for simply supported plates based on the linear third-order theory and non-linear static and dynamic finite element results based on the first-order theory were presented to show effects of volume fractions and modulus ratio of the constituents on deflections and transverse shear stresses.

In comparison to existing publications, this paper has been able to give unique contributions to the subject matter. These contributions include Mindlin-type element formulation based on averaging of transverse shear distribution over plate thickness using Lagrangian interpolation, finite strain modelling based on Green's strain-displacement equation and smooth fibre distribution technique based on numerical computation of macro-mechanical properties at Gaussian quadrature points.

2 Micro-mechanics of Fibrous Composites

This section describes the micromechanics algorithm and the fibre distribution techniques such as average and smooth fibre distribution technique. The elastic and strength properties of a composite are expressed in terms of the fibre and matrix properties as described by Daniel and Ishai (1994).

2.1 Fibre Distribution Techniques

This section explains the implementation of fibre distribution in the FE code. The equation used for fibre distribution is given below.

$$V_f(\xi) = V_1 + (V_2 - V_1)\xi^p \quad (1)$$

where

$$\xi = \frac{x-x_1}{x_2-x_1}, \quad \xi = \frac{y-y_1}{y_2-y_1} \text{ or } \xi = \frac{r-r_1}{r_2-r_1}$$

V_1 = fibre volume fraction at x_1, y_1 or r_1

V_2 = fibre volume fraction at x_2, y_2 or r_2

Manual Fibre Distribution

This fibre distribution technique enables the code user to manually specify the fibre volume fraction for each element along the direction of fibre volume fraction variation.

Average Fibre Distribution

This fibre distribution technique enables the code user to either specify fibre volume fractions V_1 and V_2 or the mean fibre volume fraction \bar{V} and fibre volume fraction V_1 . These fibre volume fractions are then used in computing the fibre volume fractions at the midpoint of each element.

Smooth Fibre Distribution

This fibre distribution technique enables the code user to either specify fibre volume fractions V_1 and V_2 or the mean fibre volume fraction \bar{V} and fibre volume fraction V_1 . These fibre volume fractions are then used in computing the fibre volume fractions at each Gaussian quadrature point.

The plots of the fibre volume fraction distribution for all ten optimisation cases considered in this paper were obtained using Eq.1 and they are as shown below.

2.2 Progressive Damage Analysis Algorithm

In this section, a progressive damage analysis algorithm has been presented. This algorithm actually contains two types of non-linearity which are finite strain and material degradation. In the case of finite strain, the geometrical non-linearity during loading is modelled by applying load incrementally as shown in the figure below. In the case of material non-linearity, during each load increment a check for failure is undertaken using an interactive failure criterion. If failure is detected, material properties of failed element are degraded and equilibrium is re-established. In this paper the failure criteria employed include Tsai-Hill, Tsai-Wu and Hoffman failure criteria. Further details on the criteria and different progressive damage techniques can be found in these references [Sleight (1999), Razzaq and El-Zafrany (2005), Prusty et. al. (2001), Padhi et. al. (1998), Tolson and Zabararas (1991), Crisfield et. al. (1997)].

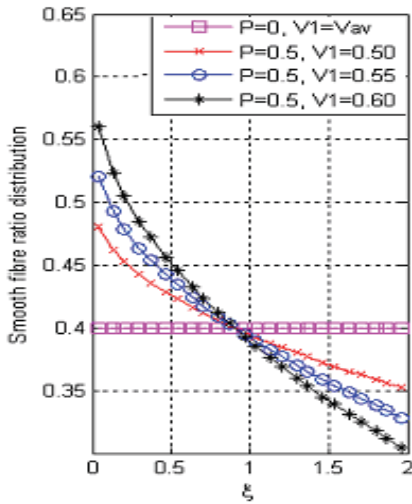


Figure 1: Smooth fibre ratio distribution plot for cases with $P=0$ and $P=0.5$

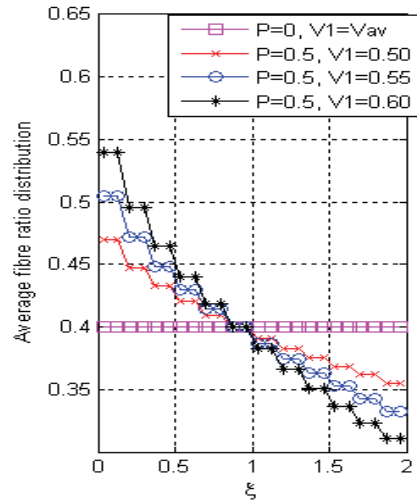


Figure 2: Average fibre ratio distribution plot for cases with $P=0$ and $P=0.5$

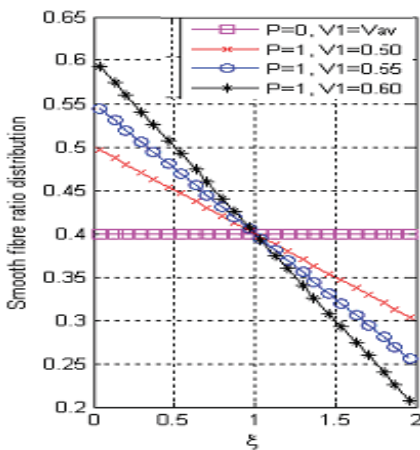


Figure 3: Smooth fibre ratio distribution plot for cases with $P=0$ and $P=1$

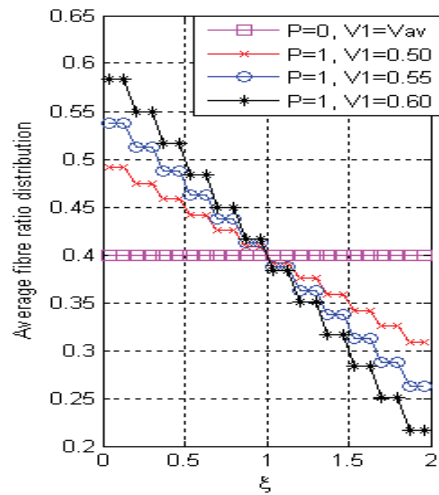


Figure 4: Average fibre ratio distribution plot for cases with $P=0$ and $P=1$

3 Derivation of Finite Element Equations

This section explains the Mindlin-type plate bending element theory and derives the equation used in the finite element programming. The finite element formulation

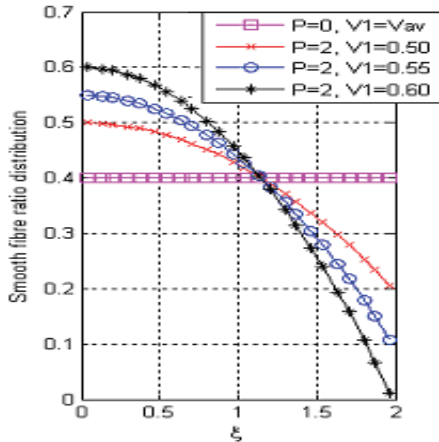


Figure 5: Smooth fibre ratio distribution plot for cases with $P=0$ and $P=2$

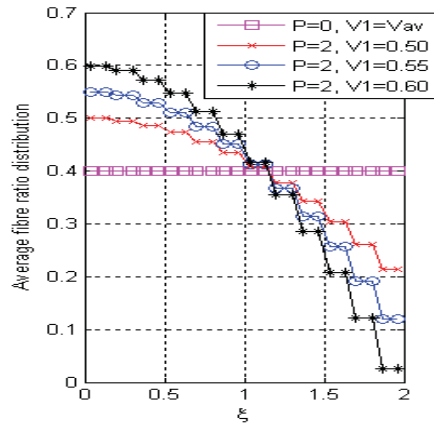


Figure 6: Average fibre ratio distribution plot for cases with $P=0$ and $P=2$

of displacement equation, strain equation, stress equation, strain energy variation and generalised equation of equilibrium have been summarised in this section. The generalised equation of equilibrium is then linearised in-order to obtain the Mindlin-type element equation.

3.1 Displacement, Stress and Strain Equations

3.1.1 Displacement Components

Using Mindlin's plate bending theory, the displacement components in the x , y and z directions at any point (x, y, z) inside the plate are as described in the following equations.

$$u(x, y, z) = u^o(x, y) + z\theta_y(x, y) \quad (2)$$

$$v(x, y, z) = v^o(x, y) - z\theta_x(x, y) \quad (3)$$

$$w(x, y, z) \approx w(x, y) \quad (4)$$

where u^o, v^o represent displacement values at the mid-plane of the plate and θ_x, θ_y are average slope angles defined as follows:

$$\theta_x = +[w_y - \bar{\gamma}_{yz}], \quad \theta_y = -[w_x - \bar{\gamma}_{xz}] \quad (5)$$

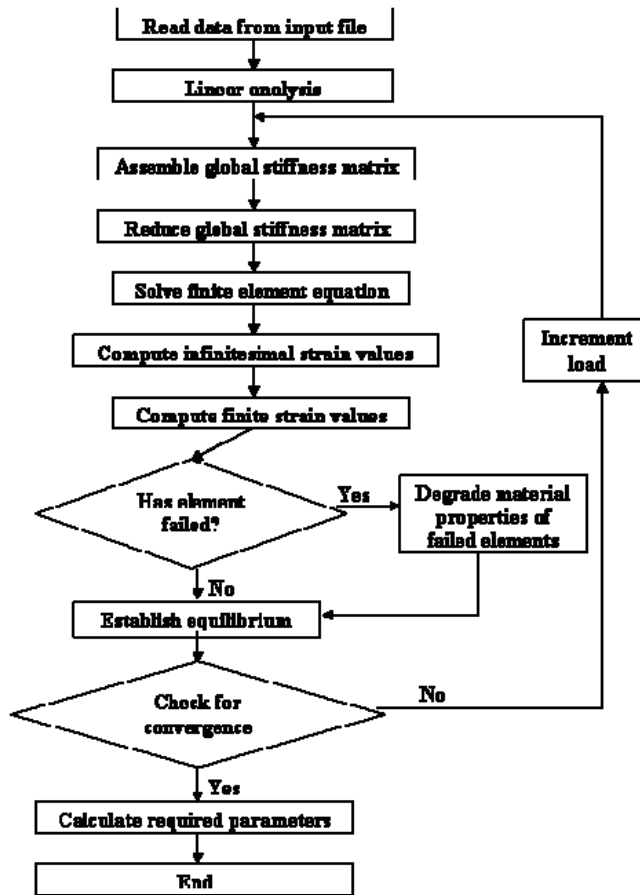


Figure 7: Progressive damage analysis algorithm

3.1.2 Strain Components

The transverse strain components at any point inside the plate are assumed infinitesimal, they are negligible for thin plates, other components are defined in the $x - y$ plane and they may assume finite values. The strain component ε_z will always be assumed negligible.

Transverse shear strains

Using Reissner's theory, the transverse shear strains at any point (x,y,z) inside the plate can be modelled as a parabolic distribution over the plate thickness as shown

in the following equation.

$$\boldsymbol{\gamma} = \begin{bmatrix} \gamma_{xz} \\ \gamma_{yz} \end{bmatrix} \equiv \frac{3}{2} \left(1 - \frac{4z^2}{h^2} \right) \begin{bmatrix} \bar{\gamma}_{xz} \\ \bar{\gamma}_{yz} \end{bmatrix} \quad (6)$$

where $\bar{\gamma}_{xz}$, $\bar{\gamma}_{yz}$ represents the average transverse shear strains over the plate thickness.

The x-y strain components

The x-y strain component contains ε_x , ε_y and γ_{xy} . Using Green's strain-displacement equations, then:

$$\varepsilon_x = u_x + 0.5 [u_x^2 + v_x^2 + w_x^2] \quad (7)$$

$$\varepsilon_y = u_y + 0.5 [u_y^2 + v_y^2 + w_y^2] \quad (8)$$

$$\gamma_{xy} = u_y + v_x + [u_x u_y + v_x v_y + w_x w_y] \quad (9)$$

where (u_x, v_x, w_x) represents the displacement derivative with respect to x and (u_y, v_y, w_y) represents the displacement derivative with respect to y.

Using the previous equations, the x-y strain vector can be partitioned as follows:

$$\begin{bmatrix} \varepsilon_x \\ \varepsilon_y \\ \gamma_{xy} \end{bmatrix} = \varepsilon_o - z\varepsilon_b + \frac{1}{2} \begin{bmatrix} A_m - zA_\theta \\ A_w \\ -zA_m + z^2A_\theta \end{bmatrix}^T \begin{bmatrix} \theta_m \\ \theta_w \\ \theta_\theta \end{bmatrix} \quad (10)$$

Hence it can be shown that:

$$\boldsymbol{\theta}_m(x, y) = [u_x^o \quad v_x^o \quad u_y^o \quad v_y^o]^T \quad (11)$$

$$\boldsymbol{\theta}_w(x, y) = [w_x \quad w_y]^T \quad (12)$$

$$\boldsymbol{\theta}_\theta(x, y) = [-(\theta_y)_x \quad (\theta_x)_x \quad -(\theta_y)_y \quad (\theta_x)_y]^T \quad (13)$$

$$\mathbf{A}_m(x, y) = \begin{bmatrix} u_x^o & v_x^o & 0 & 0 \\ 0 & 0 & u_y^o & v_y^o \\ u_y^o & v_y^o & u_x^o & v_x^o \end{bmatrix} \quad (14)$$

$$\mathbf{A}_w(x, y) = \begin{bmatrix} w_x & 0 \\ 0 & w_y \\ w_y & w_y \end{bmatrix} \quad (15)$$

$$\mathbf{A}_\theta(x, y) = \begin{bmatrix} -(\theta_y)_x & (\theta_x)_x & 0 & 0 \\ 0 & 0 & -(\theta_y)_y & (\theta_x)_y \\ -(\theta_y)_y & (\theta_x)_y & -(\theta_y)_x & (\theta_x)_x \end{bmatrix} \quad (16)$$

$$\boldsymbol{\varepsilon}_o(x, y) = [u_x^o \quad v_y^o \quad u_y^o + v_x^o]^T \quad (17)$$

$$\boldsymbol{\varepsilon}_b(x, y) = [-(\theta_y)_x \quad (\theta_x)_y \quad (\theta_x)_x - (\theta_y)_y]^T \quad (18)$$

where subscript x and y represents the derivatives with respect to x and y respectively.

Also the variation of the total $x - y$ strain vector can be represented in matrix form as shown below:

$$\begin{bmatrix} d\varepsilon_x \\ d\varepsilon_y \\ d\gamma_{xy} \end{bmatrix} = d\varepsilon_o - zd\varepsilon_b + \begin{bmatrix} A_m - zA_\theta \\ A_w \\ -zA_m + z^2A_\theta \end{bmatrix}^T \begin{bmatrix} d\theta_m \\ d\theta_w \\ d\theta_\theta \end{bmatrix} \quad (19)$$

And the variation of the transverse shear strain vector is derived from Eq.6 as:

$$d\boldsymbol{\gamma} = f_\gamma(z)d\hat{\boldsymbol{\gamma}} \quad (20)$$

where

$$\hat{\boldsymbol{\gamma}} = \begin{bmatrix} \bar{\gamma}_{xz} \\ \bar{\gamma}_{yz} \end{bmatrix} \equiv \begin{bmatrix} \frac{\partial w}{\partial x} + \theta_y \\ \frac{\partial w}{\partial y} - \theta_x \end{bmatrix} \quad (21)$$

$$f_\gamma(z) = \frac{3}{2} \left(1 - \frac{4z^2}{h^2} \right) \quad (22)$$

3.1.3 Stress Components

The relevant stress components at any point inside the l^{th} layer of a composite layered plate can be represented in terms of the transverse shear stress vector and x-y stress vector. The transverse shear stress vector $\boldsymbol{\tau}^{(l)}$ contains τ_{xz} and τ_{yz} . The x-y stress vector $\boldsymbol{\sigma}^{(l)}$ contains σ_x and σ_y . Using the constitutive equations for the l^{th} layer, the stress vectors can be expressed in terms of strain vectors as follows:

$$\boldsymbol{\tau}^{(l)} = \boldsymbol{\mu}^{(l)}\boldsymbol{\gamma} \equiv f_\gamma(z)\boldsymbol{\mu}^{(l)}\hat{\boldsymbol{\gamma}} \quad (23)$$

$$\boldsymbol{\sigma}^{(l)} = \mathbf{D}^{(l)}\boldsymbol{\varepsilon} \quad (24)$$

3.1.4 Strain Energy Variation

The variation of strain energy density (strain energy per unit volume) due to a variation of displacement at any point inside the l^{th} layer of the plate can be expressed as follows:

$$d\bar{U}^{(l)} = \sigma_x^{(l)}d\varepsilon_x + \sigma_y^{(l)}d\varepsilon_y + \tau_{xy}^{(l)}d\gamma_{xy} + \tau_{yz}^{(l)}d\gamma_{yz} + \tau_{xz}^{(l)}d\gamma_{xz} \quad (25)$$

which can be represented in the following matrix form:

$$d\bar{U}^{(l)} = d\hat{\gamma}^t \boldsymbol{\tau}^{(l)} + d\boldsymbol{\varepsilon}^t \boldsymbol{\sigma}^{(l)} \quad (26)$$

The variation of strain energy per unit area of the plate surface is defined as follows:

$$dU' = \int_{-h/2}^{h/2} (d\bar{U}^{(l)}) dz \quad (27)$$

and the variation of the strain energy of the plate is given by:

$$dU = \iint_{x-y \text{ surface}} (dU') dx dy \quad (28)$$

Substituting from Eq.19 and Eq.20 into Eq.25, it can be deduced that:

$$d\bar{U}^{(l)} = f_\gamma(z) d\hat{\gamma}^t \boldsymbol{\tau}^{(l)} + [d\boldsymbol{\varepsilon}_o + \mathbf{A}_m d\boldsymbol{\theta}_m + \mathbf{A}_w d\boldsymbol{\theta}_w - z(d\boldsymbol{\varepsilon}_b + \mathbf{A}_m d\boldsymbol{\theta}_\theta + \mathbf{A}_\theta d\boldsymbol{\theta}_m) + z^2 \mathbf{A}_\theta d\boldsymbol{\theta}_\theta] \boldsymbol{\sigma}^{(l)} \quad (29)$$

i.e.

$$d\bar{U}^{(l)} = f_\gamma(z) d\hat{\gamma}^t \boldsymbol{\tau}^{(l)} + [d\boldsymbol{\varepsilon}_o^t + d\boldsymbol{\theta}_m^t \mathbf{A}_m^t + d\boldsymbol{\theta}_w^t \mathbf{A}_w^t - z(d\boldsymbol{\varepsilon}_b^t + d\boldsymbol{\theta}_\theta^t \mathbf{A}_m^t + d\boldsymbol{\theta}_m^t \mathbf{A}_\theta^t) + z^2 d\boldsymbol{\theta}_\theta^t \mathbf{A}_\theta] \boldsymbol{\sigma}^{(l)} \quad (30)$$

3.2 Interpolated Equations

3.2.1 Displacement Components

Mindlin-type elements are based on Lagrangian interpolation, and for an n -node element the mid-plane displacement components and average slope angles at any point (x, y) in the mid-plane of the plate can be expressed in terms of nodal displacements $u_i, v_i, w_i, (\theta_x)_i, (\theta_y)_i$ and Lagrangian shape functions $N_i(x, y)$. The subscript i represents the node number.

Usually, the two-dimensional Lagrangian shape functions are expressed in terms of intrinsic coordinates (ξ, η) and the relationships between Cartesian coordinates (x, y) and intrinsic coordinates (ξ, η) are obtained via isoparametric equations as described by Attia and El-Zafrany (1999).

3.2.2 Strain Components

Transverse shear strains

Substituting the interpolated displacement components into Eq.21 and subsequently into Eq.6 to obtain:

$$\boldsymbol{\gamma}(x, y, z) = f_\gamma(z) \mathbf{B}_\gamma(x, y) \boldsymbol{\delta}_b \quad (31)$$

where \mathbf{B}_γ is the matrix containing the Lagrangian shape functions and their derivatives.

Total strain vector and its variation

The total strain vector can be represented in terms of nodal parameters as:

$$\begin{bmatrix} \varepsilon_x \\ \varepsilon_y \\ \gamma_{xy} \end{bmatrix} = \begin{bmatrix} B_o + \frac{1}{2}A_m G_m - \frac{z}{2}A_\theta G_m \\ \frac{1}{2}A_w G_w - z(B_b + \frac{1}{2}A_m G_\theta) + \frac{z^2}{2}A_\theta G_\theta \end{bmatrix}^T \begin{bmatrix} \delta_o \\ \delta_b \end{bmatrix} \quad (32)$$

Also the variation of transverse shear strains can be obtained from Eq.31 as follows:

$$d\boldsymbol{\gamma}(x, y, z) = f_\gamma(z) \mathbf{B}_\gamma(x, y) d\boldsymbol{\delta}_b \quad (33)$$

where \mathbf{B} and \mathbf{G} represents the matrices which contain the Lagrangian shape function derivatives.

Also the variation of the $x - y$ strain vector can be represented in terms of nodal parameters as shown below:

$$\begin{bmatrix} d\varepsilon_x \\ d\varepsilon_y \\ d\gamma_{xy} \end{bmatrix} = \begin{bmatrix} B_o + A_m G_m - zA_\theta G_m \\ A_w G_w - z(B_b + A_m G_\theta) + z^2 A_\theta G_\theta \end{bmatrix}^T \begin{bmatrix} d\delta_o \\ d\delta_b \end{bmatrix} \quad (34)$$

Define the following non-linear \mathbf{B} matrices:

$$\mathbf{B}_{pq} = \mathbf{A}_p \mathbf{G}_q \quad (35)$$

with $p \equiv m, w, \theta$, $q \equiv m, w, \theta$.

Define also:

$$\tilde{\mathbf{B}}_o = \mathbf{B}_o + \mathbf{A}_m \mathbf{G}_m \equiv \mathbf{B}_o + \mathbf{B}_{mm} \quad (36)$$

and

$$\tilde{\mathbf{B}}_b = \mathbf{B}_b + \mathbf{A}_m \mathbf{G}_\theta \equiv \mathbf{B}_b + \mathbf{B}_{m\theta} \quad (37)$$

Hence, Eq.34 can be rewritten as follows:

$$\begin{bmatrix} d\varepsilon_x \\ d\varepsilon_y \\ d\gamma_{xy} \end{bmatrix} = \begin{bmatrix} \tilde{\mathbf{B}}_o - z\mathbf{B}_{\theta m} \\ B_{ww} - z\tilde{\mathbf{B}}_b + z^2 \mathbf{B}_{\theta\theta} \end{bmatrix}^T \begin{bmatrix} d\delta_o \\ d\delta_b \end{bmatrix} \quad (38)$$

3.2.3 Variation of Strain Energy

Substituting Eq.33 and Eq.34 into Eq.26, then the variation of strain energy density at any point inside the l^{th} layer of the plate can be expressed as follows:

$$d\bar{U}^{(l)}(x,y,z) = [d\delta_b^t \mathbf{B}_\gamma^t] \left(f_\gamma(z) \boldsymbol{\tau}^{(l)} \right) + \begin{bmatrix} d\delta_o \\ d\delta_b \end{bmatrix}^T \begin{bmatrix} B_o^t + G_m^t A_m^t - z G_m^t A_\theta^t \\ G_w^t A_w^t - z (B_b^t + G_\theta^t A_m^t) + z^2 G_\theta^t A_\theta^t \end{bmatrix}^T \boldsymbol{\sigma}^{(l)} \quad (39)$$

Integrated stress vectors

(a) *Integrated transverse shear stress*

This is defined as follows:

$$\tilde{\boldsymbol{\tau}} = \int_{-h/2}^{h/2} f_\gamma(z) \boldsymbol{\tau}^{(l)} dz \quad (40)$$

Substituting from Eq.23 into Eq.40, then it can be deduced that:

$$\tilde{\boldsymbol{\tau}} = \left[\int_{-h/2}^{h/2} f_\gamma^2(z) \boldsymbol{\mu}^{(l)} dz \right] \hat{\boldsymbol{\gamma}} \quad (41)$$

Define an integrated $\boldsymbol{\mu}$ matrix as follows:

$$\boldsymbol{\mu}_{\gamma\gamma} = \int_{-h/2}^{h/2} f_\gamma^2(z) \boldsymbol{\mu}^{(l)} dz \equiv \int_{-h/2}^{h/2} \frac{9}{4} \left(1 - \frac{4z^2}{h^2} \right)^2 \boldsymbol{\mu}^{(l)} dz \quad (42)$$

and for the special case of transversely isotropic plate, where all layers have the same $\boldsymbol{\mu}$ matrix, it can be proved that:

$$\boldsymbol{\mu}_{\gamma\gamma} = \frac{6}{5} h \boldsymbol{\mu} \quad (43)$$

Hence, it can be deduced that:

$$\tilde{\boldsymbol{\tau}} = \boldsymbol{\mu}_{\gamma\gamma} \hat{\boldsymbol{\gamma}} \equiv \boldsymbol{\mu}_{\gamma\gamma} \mathbf{B}_\gamma \boldsymbol{\delta}_b \quad (44)$$

(b) *Integrated x-y stress vectors*

These can be defined generally as follows:

$$\boldsymbol{\sigma}_n = (-1)^n \int_{-h/2}^{h/2} z^n \boldsymbol{\sigma}^{(l)} dz \quad (45)$$

Eq.45 can also be expressed as:

$$\boldsymbol{\sigma}_n = (-1)^n [\mathbf{D}_n (\boldsymbol{\varepsilon}_o + \boldsymbol{\varepsilon}_m + \boldsymbol{\varepsilon}_w) - \mathbf{D}_{n+1} (\boldsymbol{\varepsilon}_b + \boldsymbol{\varepsilon}_{m\theta}) + \mathbf{D}_{n+2} \boldsymbol{\varepsilon}_\theta] \quad (46)$$

Defining integrated \mathbf{D} matrices generally as follows:

$$\mathbf{D}_n = \int_{-h/2}^{h/2} z^n \mathbf{D}^{(l)} dz \quad (47)$$

Integrating Eq.39 over the layers with respect to z , then it can be deduced that:

$$dU^{(l)} = d\boldsymbol{\delta}'_b \mathbf{B}'_\gamma \tilde{\boldsymbol{\tau}} + (d\boldsymbol{\delta}'_o \tilde{\mathbf{B}}'_o + d\boldsymbol{\delta}'_b \mathbf{B}'_{ww}) \boldsymbol{\sigma}_o + (d\boldsymbol{\delta}'_o \mathbf{B}'_{\theta m} + d\boldsymbol{\delta}'_b \tilde{\mathbf{B}}'_b) \boldsymbol{\sigma}_1 + d\boldsymbol{\delta}'_b \mathbf{B}'_{\theta\theta} \boldsymbol{\sigma}_2 \quad (48)$$

3.3 Finite Element Equations

3.3.1 Generalized Equations of Equilibrium

The work done by actual external loads can be expressed in terms of equivalent nodal loading represented with the following vector:

$$\mathbf{F} \equiv \begin{bmatrix} \mathbf{F}_o \\ \mathbf{F}_b \end{bmatrix} \quad (49)$$

where

$$\mathbf{F}_o = \{(F_x)_1 \quad (F_y)_1 \quad (F_x)_2 \quad (F_y)_2 \quad \cdots \quad (F_x)_m \quad (F_y)_m\} \quad (50)$$

$$\mathbf{F}_b = \{(F_z)_1 \quad (M_x)_1 \quad (M_y)_1 \quad \cdots \quad (F_z)_m \quad (M_x)_m \quad (M_y)_m\} \quad (51)$$

and m is the total number of finite element mesh nodes.

From the principle of virtual work due to a variation of displacement:

$$d\chi = dU - dW = 0 \quad (52)$$

Eq.52 can be expressed as:

$$\sum_{e=1}^{N_e} \int_{-h/2}^{h/2} \iint_e \left\{ \begin{bmatrix} d\delta_o \\ d\delta_b \end{bmatrix}^T \begin{bmatrix} B_o^t + G_m^t A_m^t - z G_m^t A_\theta^t \\ G_w^t A_w^t - z(B_b^t + G_\theta^t A_m^t) + z^2 G_\theta^t A_\theta^t \end{bmatrix} \sigma^{(L)} + d\delta_b^t B_\gamma^t f_\gamma \tau^{(L)} \right\} dx dy dz - d\delta_o^t F_o^t - d\delta_b^t F_b^t = 0 \quad (53)$$

Since $d\delta_o, d\delta_b$ represent arbitrary parameters, then their coefficients in the above equation vanish, leading to:

$$\sum_{e=1}^{N_e} \int_{-h/2}^{h/2} \iint_e \left\{ \begin{bmatrix} B_o^t + G_m^t A_m^t - z G_m^t A_\theta^t \\ G_w^t A_w^t - z(B_b^t + G_\theta^t A_m^t) + z^2 G_\theta^t A_\theta^t \end{bmatrix} \sigma^{(L)} + B_\gamma^t f_\gamma \tau^{(L)} \right\} dx dy dz - [F_o \quad F_b]^T = 0 \quad (54)$$

which represent the generalized equations of equilibrium.

If an approximate solution is employed then the previous equations will lead to the following residual vectors:

$$\sum_{e=1}^{N_e} \int_{-h/2}^{h/2} \iint_e \left\{ \begin{bmatrix} B_o^t + G_m^t A_m^t - z G_m^t A_\theta^t \\ G_w^t A_w^t - z(B_b^t + G_\theta^t A_m^t) + z^2 G_\theta^t A_\theta^t \end{bmatrix} \sigma^{(L)} + B_\gamma^t f_\gamma \tau^{(L)} \right\} dx dy dz - [F_o \quad F_b]^T = [R_o \quad R_b]^T \quad (55)$$

When calculating the residual forces, the equation above is integrated analytically with respect to z , leading to:

$$\mathbf{R}_o = \mathbf{F}_o - \sum_{e=1}^{N_e} \iint_e \{ (\mathbf{B}_o^t + \mathbf{G}_m^t \mathbf{A}_m^t) \sigma_0 + (\mathbf{G}_m^t \mathbf{A}_\theta^t) \sigma_1 \} dx dy \quad (56)$$

$$\mathbf{R}_b = \mathbf{F}_b - \sum_{e=1}^{N_e} \iint_e \{ \mathbf{B}_\gamma^t \tilde{\tau} + (\mathbf{G}_w^t \mathbf{A}_w^t) \sigma_0 + (\mathbf{B}_b^t + \mathbf{G}_\theta^t \mathbf{A}_m^t) \sigma_1 + (\mathbf{G}_\theta^t \mathbf{A}_\theta^t) \sigma_2 \} dx dy \quad (57)$$

3.3.2 Linearization of Equations of Equilibrium

To restore equilibrium, i.e. to make the residual vectors vanish we assume:

$$\begin{aligned} \delta_{new} &= \delta_{old} + \Delta \delta \\ \sigma_{new}^{(l)} &= \sigma_{old}^{(l)} + \Delta \sigma \\ \mathbf{A}_{new} &= \mathbf{A}_{old} + \Delta \mathbf{A} \end{aligned} \quad (58)$$

such that $\mathbf{R}_o \rightarrow \mathbf{O}$, $\mathbf{R}_b \rightarrow \mathbf{O}$.

Substituting Eq.58 into Eq.55, then it can be deduced that:

$$\sum_{e=1}^{N_e} \iiint_e \left\{ [\mathbf{B}_o^t + \mathbf{G}_m^t (\mathbf{A}_m^t + \Delta \mathbf{A}_m^t)] (\boldsymbol{\sigma}^{(l)} + \Delta \boldsymbol{\sigma}^{(l)}) + \mathbf{G}_m^t (\mathbf{A}_\theta^t + \Delta \mathbf{A}_\theta^t) (-z) (\boldsymbol{\sigma}^{(l)} + \Delta \boldsymbol{\sigma}^{(l)}) \right\} dx dy dz - \mathbf{F}_o = \mathbf{O} \quad (59)$$

$$\sum_{e=1}^{N_e} \iiint_e \left\{ \mathbf{B}_\gamma^t f_\gamma(z) (\boldsymbol{\tau}^{(l)} + \Delta \boldsymbol{\tau}^{(l)}) + \mathbf{G}_w^t (\mathbf{A}_w^t + \Delta \mathbf{A}_w^t) (\boldsymbol{\sigma}^{(l)} + \Delta \boldsymbol{\sigma}^{(l)}) + [\mathbf{B}_b^t + \mathbf{G}_\theta^t (\mathbf{A}_m^t + \Delta \mathbf{A}_m^t)] (-z) (\boldsymbol{\sigma}^{(l)} + \Delta \boldsymbol{\sigma}^{(l)}) + \mathbf{G}_\theta^t (\mathbf{A}_\theta^t + \Delta \mathbf{A}_\theta^t) (z^2) (\boldsymbol{\sigma}^{(l)} + \Delta \boldsymbol{\sigma}^{(l)}) \right\} dx dy dz - \mathbf{F}_b = \mathbf{O} \quad (60)$$

Expanding the previous expressions and ignoring high order terms, and using the definitions of \mathbf{R}_o , \mathbf{R}_b given in Eq.55, then Eq.59 and Eq.60 can be reduced to:

$$\sum_{e=1}^{N_e} \iiint_e \left\{ [\mathbf{B}_o^t + \mathbf{G}_m^t \mathbf{A}_m^t] \Delta \boldsymbol{\sigma}^{(l)} + \mathbf{G}_m^t \mathbf{A}_\theta^t (-z \Delta \boldsymbol{\sigma}^{(l)}) + \mathbf{G}_m^t \Delta \mathbf{A}_m^t \boldsymbol{\sigma}^{(l)} + \mathbf{G}_m^t \Delta \mathbf{A}_\theta^t (-z \boldsymbol{\sigma}^{(l)}) \right\} dx dy dz = \mathbf{R}_o \quad (61)$$

$$\sum_{e=1}^{N_e} \iiint_e \left\{ \mathbf{B}_\gamma^t f_\gamma(z) \Delta \boldsymbol{\tau}^{(l)} + \mathbf{G}_w^t \mathbf{A}_w^t \Delta \boldsymbol{\sigma}^{(l)} + [\mathbf{B}_b^t + \mathbf{G}_\theta^t \mathbf{A}_m^t] (-z \Delta \boldsymbol{\sigma}^{(l)}) + \mathbf{G}_\theta^t \mathbf{A}_\theta^t (z^2 \Delta \boldsymbol{\sigma}^{(l)}) + \mathbf{G}_w^t \Delta \mathbf{A}_w^t \boldsymbol{\sigma}^{(l)} + \mathbf{G}_\theta^t \Delta \mathbf{A}_m^t (-z) \boldsymbol{\sigma}^{(l)} + \mathbf{G}_\theta^t \Delta \mathbf{A}_\theta^t (z^2) \boldsymbol{\sigma}^{(l)} \right\} dx dy dz = \mathbf{R}_b \quad (62)$$

Eq.61 and Eq.62 can be divided into two parts each. The first part contains the terms which include $\Delta \boldsymbol{\sigma}$ and the second part has the terms with $\Delta \mathbf{A}$'s, as follows:

$$\sum_{e=1}^{N_e} [(\mathbf{R}_i^e)_{\Delta \boldsymbol{\sigma}} + (\mathbf{R}_i^e)_{\Delta \mathbf{A}}] = \mathbf{R}_i \quad (63)$$

with $i = o, b$.

Using the non-linear \mathbf{B} matrices, it can be shown that

$$(\mathbf{R}_o^e)_{\Delta \boldsymbol{\sigma}} = \int_{-h/2}^{h/2} \iint_e \left[\tilde{\mathbf{B}}_o^t \Delta \boldsymbol{\sigma}^{(l)} + \mathbf{B}_{\theta m}^t (-z \Delta \boldsymbol{\sigma}^{(l)}) \right] dx dy dz \quad (64)$$

$$(\mathbf{R}_b^e)_{\Delta\sigma} = \int_{-h/2}^{h/2} \iint_e \left[\mathbf{B}_\gamma^t f_\gamma(z) \Delta\boldsymbol{\tau}^{(l)} + \mathbf{B}_{ww}^t \Delta\boldsymbol{\sigma}^{(l)} + \tilde{\mathbf{B}}_b^t (-z \Delta\boldsymbol{\sigma}^{(l)}) + \mathbf{B}_{\theta\theta}^t (z^2 \Delta\boldsymbol{\sigma}^{(l)}) \right] dx dy dz \quad (65)$$

$$(\mathbf{R}_o^e)_{\Delta\mathbf{A}} = \int_{-h/2}^{h/2} \iint_e \left[\mathbf{G}_m^t \Delta\mathbf{A}_m^t \boldsymbol{\sigma}^{(l)} + \mathbf{G}_m^t \Delta\mathbf{A}_\theta^t (-z) \boldsymbol{\sigma}^{(l)} \right] dx dy dz \quad (66)$$

$$(\mathbf{R}_b^e)_{\Delta\mathbf{A}} = \int_{-h/2}^{h/2} \iint_e \left[\mathbf{G}_w^t \Delta\mathbf{A}_w^t \boldsymbol{\sigma}^{(l)} + \mathbf{G}_\theta^t \Delta\mathbf{A}_m^t (-z) \boldsymbol{\sigma}^{(l)} + \mathbf{G}_\theta^t \Delta\mathbf{A}_\theta^t (z^2) \boldsymbol{\sigma}^{(l)} \right] dx dy dz \quad (67)$$

3.3.3 Analysis of $\Delta\boldsymbol{\sigma}$ Terms

Using Eq.23 and Eq.31, the increment of transverse shear stress can be expressed as follows:

$$\Delta\boldsymbol{\tau}^{(l)} = f_\gamma(z) \boldsymbol{\mu}^{(l)} \Delta\hat{\boldsymbol{\gamma}} \equiv f_\gamma(z) \boldsymbol{\mu}^{(l)} \mathbf{B}_\gamma \Delta\boldsymbol{\delta}_b \quad (68)$$

Hence, it can be deduced that:

$$\int_{-h/2}^{h/2} f_\gamma(z) \Delta\boldsymbol{\tau}^{(l)} dz = \boldsymbol{\mu}_{\gamma\gamma} \mathbf{B}_\gamma \Delta\boldsymbol{\delta}_b \quad (69)$$

Similarly the increment of $x - y$ stress can be obtained from Eq.24 and Eq.38, as follows:

$$\Delta\boldsymbol{\sigma}^{(l)} = \mathbf{D}^{(l)} \Delta\boldsymbol{\varepsilon} \equiv \mathbf{D}^{(l)} \left[\tilde{\mathbf{B}}_o \Delta\boldsymbol{\delta}_o + \mathbf{B}_{ww} \Delta\boldsymbol{\delta}_b - z (\mathbf{B}_{\theta m} \Delta\boldsymbol{\delta}_o + \tilde{\mathbf{B}}_b \Delta\boldsymbol{\delta}_b) + z^2 \mathbf{B}_{\theta\theta} \Delta\boldsymbol{\delta}_b \right] \quad (70)$$

Using Eq.46, the following integrated stress increments can be deduced:

$$\int_{-h/2}^{h/2} \Delta\boldsymbol{\sigma}^{(l)} dz = \mathbf{D}_o (\tilde{\mathbf{B}}_o \Delta\boldsymbol{\delta}_o + \mathbf{B}_{ww} \Delta\boldsymbol{\delta}_b) - \mathbf{D}_1 (\mathbf{B}_{\theta m} \Delta\boldsymbol{\delta}_o + \tilde{\mathbf{B}}_b \Delta\boldsymbol{\delta}_b) + \mathbf{D}_2 (\mathbf{B}_{\theta\theta} \Delta\boldsymbol{\delta}_b) \quad (71)$$

$$\int_{-h/2}^{h/2} z \Delta\boldsymbol{\sigma}^{(l)} dz = \mathbf{D}_1 (\tilde{\mathbf{B}}_o \Delta\boldsymbol{\delta}_o + \mathbf{B}_{ww} \Delta\boldsymbol{\delta}_b) - \mathbf{D}_2 (\mathbf{B}_{\theta m} \Delta\boldsymbol{\delta}_o + \tilde{\mathbf{B}}_b \Delta\boldsymbol{\delta}_b) + \mathbf{D}_3 (\mathbf{B}_{\theta\theta} \Delta\boldsymbol{\delta}_b)$$

(72)

$$\int_{-h/2}^{h/2} z^2 \Delta \boldsymbol{\sigma}^{(l)} dz = \mathbf{D}_2 (\tilde{\mathbf{B}}_o \Delta \boldsymbol{\delta}_o + \mathbf{B}_{ww} \Delta \boldsymbol{\delta}_b) - \mathbf{D}_3 (\mathbf{B}_{\theta m} \Delta \boldsymbol{\delta}_o + \tilde{\mathbf{B}}_b \Delta \boldsymbol{\delta}_b) + \mathbf{D}_4 (\mathbf{B}_{\theta \theta} \Delta \boldsymbol{\delta}_b) \quad (73)$$

Using Eq.69 and Eq.71 – Eq.73 then Eq.64 and Eq.65 can be reduced as follows:

$$(\mathbf{R}_o^e)_{\Delta \boldsymbol{\sigma}} = \mathbf{K}_{oo} \Delta \boldsymbol{\delta}_o + \mathbf{K}_{ob} \Delta \boldsymbol{\delta}_b \quad (74)$$

$$(\mathbf{R}_b^e)_{\Delta \boldsymbol{\sigma}} = \mathbf{K}_{bo} \Delta \boldsymbol{\delta}_o + \mathbf{K}_{bb} \Delta \boldsymbol{\delta}_b + \mathbf{K}_{\gamma \gamma} \Delta \boldsymbol{\delta}_b \quad (75)$$

where

$$\mathbf{K}_{oo} = \iint_e \left[\tilde{\mathbf{B}}_o^t \mathbf{D}_o \tilde{\mathbf{B}}_o - \tilde{\mathbf{B}}_o^t \mathbf{D}_1 \mathbf{B}_{\theta m} - \mathbf{B}_{\theta m}^t \mathbf{D}_1 \tilde{\mathbf{B}}_o + \mathbf{B}_{\theta m}^t \mathbf{D}_2 \mathbf{B}_{\theta m} \right] dx dy \quad (76)$$

$$\mathbf{K}_{ob} = \iint_e \left[\tilde{\mathbf{B}}_o^t \mathbf{D}_o \mathbf{B}_{ww} - \tilde{\mathbf{B}}_o^t \mathbf{D}_1 \tilde{\mathbf{B}}_b - \mathbf{B}_{\theta m}^t \mathbf{D}_1 \mathbf{B}_{ww} + \tilde{\mathbf{B}}_o^t \mathbf{D}_2 \mathbf{B}_{\theta \theta} + \mathbf{B}_{\theta m}^t \mathbf{D}_2 \tilde{\mathbf{B}}_b - \mathbf{B}_{\theta m}^t \mathbf{D}_3 \mathbf{B}_{\theta \theta} \right] dx dy \quad (77)$$

$$\mathbf{K}_{bo} = \iint_e \left[\mathbf{B}_{ww}^t \mathbf{D}_o \tilde{\mathbf{B}}_o - \tilde{\mathbf{B}}_b^t \mathbf{D}_1 \tilde{\mathbf{B}}_o - \mathbf{B}_{ww}^t \mathbf{D}_1 \mathbf{B}_{\theta m} + \mathbf{B}_{\theta \theta}^t \mathbf{D}_2 \tilde{\mathbf{B}}_o + \tilde{\mathbf{B}}_b^t \mathbf{D}_2 \mathbf{B}_{\theta m} - \mathbf{B}_{\theta \theta}^t \mathbf{D}_3 \mathbf{B}_{\theta m} \right] dx dy \equiv \mathbf{K}_{ob}^t \quad (78)$$

$$\mathbf{K}_{\gamma \gamma} = \iint_e \mathbf{B}_{\gamma}^t \boldsymbol{\mu}_{\gamma \gamma} \mathbf{B}_{\gamma} dx dy \quad (79)$$

$$\mathbf{K}_{bb} = \iint_e \left[\mathbf{B}_{ww}^t \mathbf{D}_o \mathbf{B}_{ww} - \mathbf{B}_{ww}^t \mathbf{D}_1 \tilde{\mathbf{B}}_b - \tilde{\mathbf{B}}_b^t \mathbf{D}_1 \mathbf{B}_{ww} + \tilde{\mathbf{B}}_b^t \mathbf{D}_2 \tilde{\mathbf{B}}_b + \mathbf{B}_{ww}^t \mathbf{D}_2 \mathbf{B}_{\theta \theta} + \mathbf{B}_{\theta \theta}^t \mathbf{D}_2 \mathbf{B}_{ww} - \tilde{\mathbf{B}}_b^t \mathbf{D}_3 \mathbf{B}_{\theta \theta} - \mathbf{B}_{\theta \theta}^t \mathbf{D}_3 \tilde{\mathbf{B}}_b + \mathbf{B}_{\theta \theta}^t \mathbf{D}_4 \mathbf{B}_{\theta \theta} \right] dx dy \quad (80)$$

3.3.4 Analysis of ΔA Terms

Using the integrated stress defined by Eq.45, then Eq.66 and Eq.67 can be simplified as follows:

$$(\mathbf{R}_o^e)_{\Delta A} = \iint_e [\mathbf{G}_m^t \Delta \mathbf{A}_m^t \boldsymbol{\sigma}_o + \mathbf{G}_m^t \Delta \mathbf{A}_\theta^t \boldsymbol{\sigma}_1] dx dy \quad (81)$$

$$(\mathbf{R}_b^e)_{\Delta A} = \iint_e [\mathbf{G}_w^t \Delta \mathbf{A}_w^t \boldsymbol{\sigma}_o + \mathbf{G}_\theta^t \Delta \mathbf{A}_m^t \boldsymbol{\sigma}_1 + \mathbf{G}_\theta^t \Delta \mathbf{A}_\theta^t \boldsymbol{\sigma}_2] dx dy \quad (82)$$

Using matrix manipulations, the following theorems can be proved:

$$\Delta \mathbf{A}_m^t \boldsymbol{\sigma}_n \equiv \mathbf{S}_n \Delta \boldsymbol{\theta}_m = \mathbf{S}_n \mathbf{G}_m \Delta \boldsymbol{\delta}_o \quad (83)$$

$$\Delta \mathbf{A}_\theta^t \boldsymbol{\sigma}_n \equiv \mathbf{S}_n \Delta \boldsymbol{\theta}_\theta = \mathbf{S}_n \mathbf{G}_\theta \Delta \boldsymbol{\delta}_b \quad (84)$$

$$\Delta \mathbf{A}_w^t \boldsymbol{\sigma}_o \equiv \mathbf{S}_w \Delta \boldsymbol{\theta}_w = \mathbf{S}_w \mathbf{G}_w \Delta \boldsymbol{\delta}_b \quad (85)$$

where

$$\mathbf{S}_n = \begin{bmatrix} \sigma_x^{(n)} & 0 & \tau_{xy}^{(n)} & 0 \\ 0 & \sigma_x^{(n)} & 0 & \tau_{xy}^{(n)} \\ \tau_{xy}^{(n)} & 0 & \sigma_y^{(n)} & 0 \\ 0 & \tau_{xy}^{(n)} & 0 & \sigma_y^{(n)} \end{bmatrix} \quad (86)$$

and

$$\mathbf{S}_w = \begin{bmatrix} \sigma_x^{(0)} & \tau_{xy}^{(0)} \\ \tau_{xy}^{(0)} & \sigma_y^{(0)} \end{bmatrix} \quad (87)$$

Substituting from Eq.83 – Eq.85 into Eq.81 and Eq.82, then it can be deduced that:

$$(\mathbf{R}_o^e)_{\Delta A} = \mathbf{K}_{mm}^\sigma \Delta \boldsymbol{\delta}_o + \mathbf{K}_{m\theta}^\sigma \Delta \boldsymbol{\delta}_b \quad (88)$$

$$(\mathbf{R}_b^e)_{\Delta A} = \mathbf{K}_{\theta m}^\sigma \Delta \boldsymbol{\delta}_o + (\mathbf{K}_{ww}^\sigma + \mathbf{K}_{\theta\theta}^\sigma) \Delta \boldsymbol{\delta}_b \quad (89)$$

where

$$\mathbf{K}_{mm}^\sigma = \iint_e \mathbf{G}_m^t \mathbf{S}_o \mathbf{G}_m dx dy \quad (90)$$

$$\mathbf{K}_{m\theta}^\sigma = \iint_e \mathbf{G}_m^t \mathbf{S}_1 \mathbf{G}_\theta dx dy \quad (91)$$

$$\mathbf{K}_{\theta m}^{\sigma} = \iint_e \mathbf{G}_{\theta}^t \mathbf{S}_1 \mathbf{G}_m dx dy \quad (92)$$

$$\mathbf{K}_{ww}^{\sigma} = \iint_e \mathbf{G}_w^t \mathbf{S}_w \mathbf{G}_w dx dy \quad (93)$$

$$\mathbf{K}_{\theta\theta}^{\sigma} = \iint_e \mathbf{G}_{\theta}^t \mathbf{S}_2 \mathbf{G}_{\theta} dx dy \quad (94)$$

3.3.5 Final Matrix Equations of the Element

Substituting from Eq.74, Eq.75, Eq.88, Eq.89 into Eq.63, it can be deduced that:

$$\sum_{e=1}^{N_e} \{ \mathbf{K}_{oo} \Delta \boldsymbol{\delta}_o + \mathbf{K}_{ob} \Delta \boldsymbol{\delta}_b + \mathbf{K}_{mm}^{\sigma} \Delta \boldsymbol{\delta}_o + \mathbf{K}_{m\theta}^{\sigma} \Delta \boldsymbol{\delta}_b \} = \mathbf{R}_o \quad (95)$$

$$\sum_{e=1}^{N_e} \{ \mathbf{K}_{bo} \Delta \boldsymbol{\delta}_o + (\mathbf{K}_{\gamma\gamma} + \mathbf{K}_{bb}) \Delta \boldsymbol{\delta}_b + \mathbf{K}_{\theta m}^{\sigma} \Delta \boldsymbol{\delta}_o + (\mathbf{K}_{ww}^{\sigma} + \mathbf{K}_{\theta\theta}^{\sigma}) \Delta \boldsymbol{\delta}_b \} = \mathbf{R}_b \quad (96)$$

which can be rewritten as follows:

$$\sum_{e=1}^{N_e} \left\{ (\mathbf{K} + \mathbf{K}^{\sigma}) \begin{bmatrix} \Delta \boldsymbol{\delta}_o \\ \Delta \boldsymbol{\delta}_b \end{bmatrix} \right\} = \begin{bmatrix} \mathbf{R}_o \\ \mathbf{R}_b \end{bmatrix} \quad (97)$$

and the element stiffness matrices are defined as follow:

$$\mathbf{K} = \begin{bmatrix} \mathbf{K}_{oo} & \mathbf{K}_{ob} \\ \mathbf{K}_{bo} & \mathbf{K}_{bb} + \mathbf{K}_{\gamma\gamma} \end{bmatrix} \quad (98)$$

$$\mathbf{K}^{\sigma} = \begin{bmatrix} \mathbf{K}_{mm}^{\sigma} & \mathbf{K}_{m\theta}^{\sigma} \\ \mathbf{K}_{\theta m}^{\sigma} & \mathbf{K}_{ww}^{\sigma} + \mathbf{K}_{\theta\theta}^{\sigma} \end{bmatrix} \quad (99)$$

4 Finite Element Modelling and Result Validation

Composite Material Data

The composite material data used for all the cases studies are tabulated below.

A rectangular plate made of a typical FGM with its mid-plane as shown in Figure 8 was considered. A 72 element mesh was employed for all the three validation case studies. The elements used in the validation exercise include 4-noded Average Mindlin-type element, 4-noded Smooth Mindlin-type element and 4-noded Ordinary Mindlin-type element. The boundary condition applied in the three case studies is that edge $x=0$ is a clamped edge. A load of 0.1kN was applied as an equivalent nodal loading at edge $x=2$ for all load cases.

Table 1: Composite material data

Parameters	Values
E_f , Fibre young modulus	330GPa
E_m , Matrix young modulus	5GPa
ν_f , Fibre Poisson ratio	0.3625
ν_m , Matrix Poisson ratio	0.3
ρ_f , Fibre density	1.0Kg/m ³
ρ_m , Matrix density	1.0Kg/m ³
Stacking sequence	$((-45,0,45)_2)_S$
Ply thickness	2.5mm
X_{MT} , Matrix tensile strength	0.05 MPa
X_{MC} , Matrix compressive strength	0.08 MPa
X_{MS} , Matrix shear strength	0.04 MPa
X_{FT} , Fibre tensile strength	7.5 MPa
X_{FS} , Fibre shear strength	4 MPa
S_{EGRM} , Maximum radial residual stress	0.0
S_{KC} , Longitudinal stress concentration factor	1
S_{KS} , Shear stress concentration factor	1
V_1 , Fibre ratio at the clamped end	0.5, 0.55 or 0.6
\bar{V} , Average fibre ratio	0.4
P, Power term in the fibre distribution equation	0, 0.5, 1 or 2

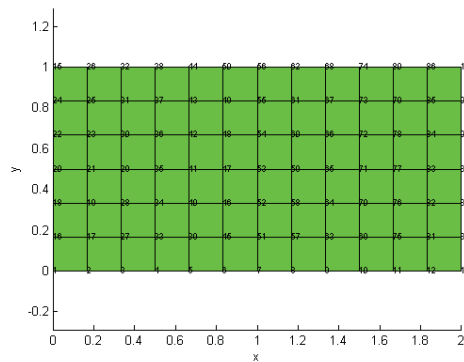


Figure 8: Mesh

4.1 Code Validation using Tension Case

Figure 9 and Figure 10 show the displacement validation results of the nodes along the axis that passes through $y=0$ and $z=0$. The in-plane displacement results for the

average, smooth and ordinary Mindlin programs were in good agreement.

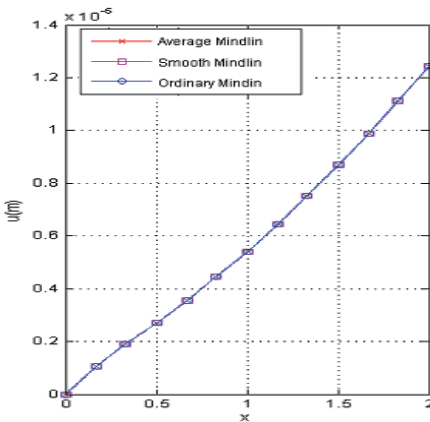


Figure 9: u-displacement validation for the tension case at the $y=0$ edge

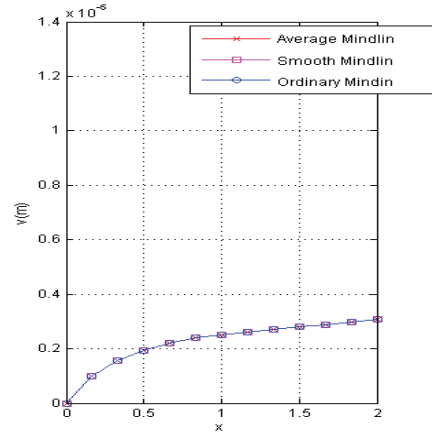


Figure 10: v-displacement validation for the tension case at the $y=0$ edge

4.2 Code Validation using Bending Case

In-plane Bending Case

Figure 11 and Figure 12 show the displacement validation results of the nodes along the axis that passes through $y=0$ and $z=0$. The in-plane displacement results for the average, smooth and ordinary Mindlin programs were in good agreement.

Out-of-plane Bending Case

Figure 13 shows the displacement validation results of the nodes along the axis that passes through $y=0$ and $z=0$. The out-of-plane displacement results for the average and ordinary Mindlin programs were in good agreement. The smooth program was not in good agreement with the other two programs. This can be explained by the fact that the smooth fibre distribution technique is a more accurate representation of the distribution equation because fibre ratios are computed at the Gaussian quadrature points of each element and not at the mid-point of each element as is the case for the average and ordinary program. Hence, it can be shown that the use of finer meshes in the average and ordinary programs brings about reduction in the result discrepancies with the smooth program.

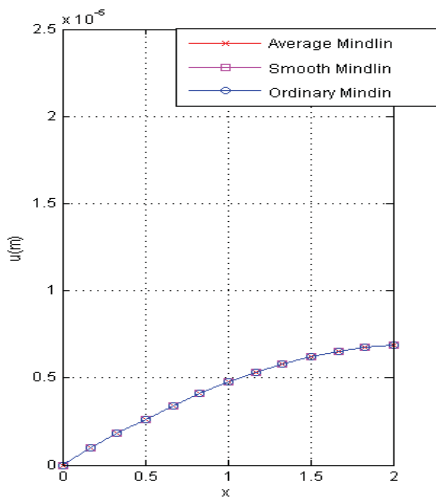


Figure 11: u-displacement validation for the in-plane bending case at the y=0 edge

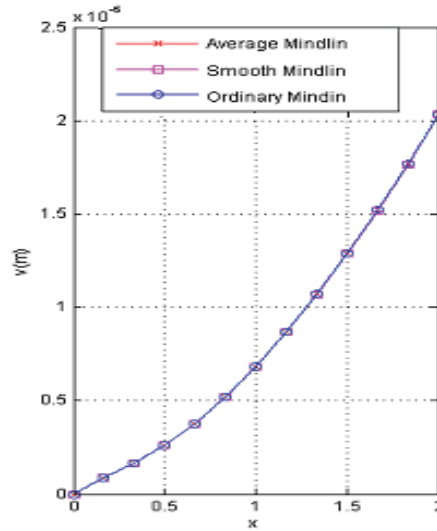


Figure 12: v-displacement validation for the in-plane bending case at the y=0 edge

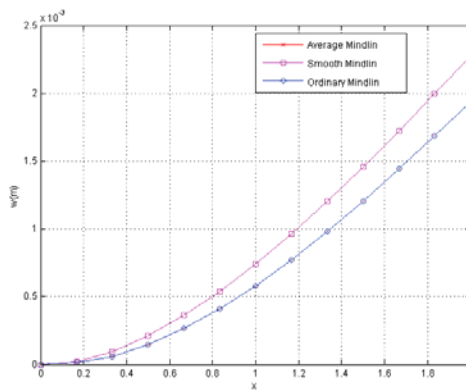


Figure 13: w-displacement validation for the out-of-plane bending case at the y=0 edge

5 Optimisation Result

The optimisation technique used in this paper can be described as a fail-safe design technique which involves the imposition of constraints to ensure that the physi-

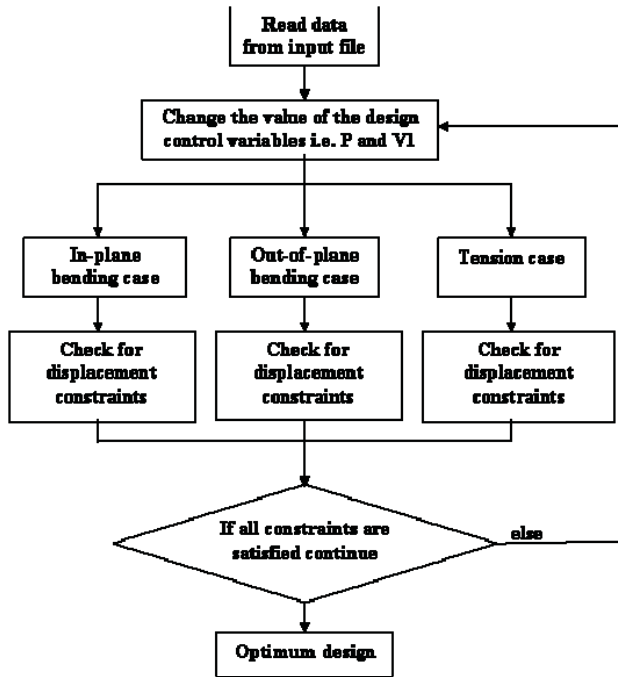


Figure 14: Optimisation technique

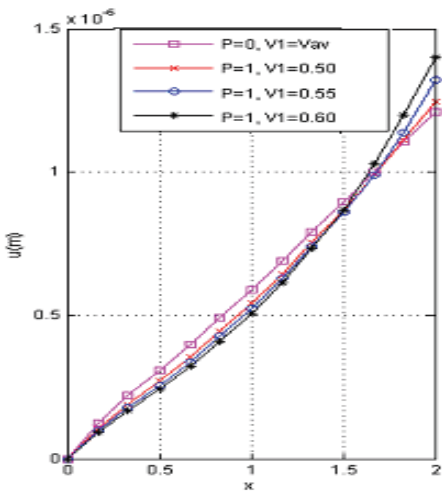


Figure 15: u-displacement result comparison for tension cases with P=0 and P=1

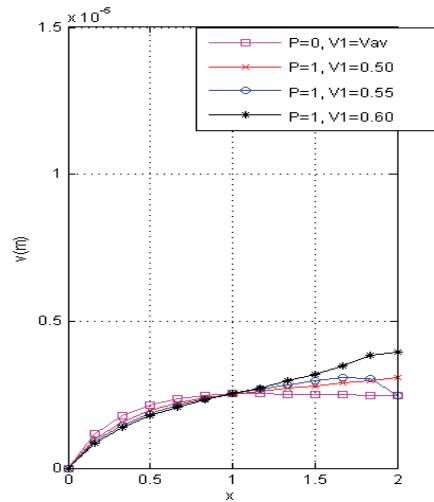


Figure 16: v-displacement result comparison for tension cases with P=0 and P=1

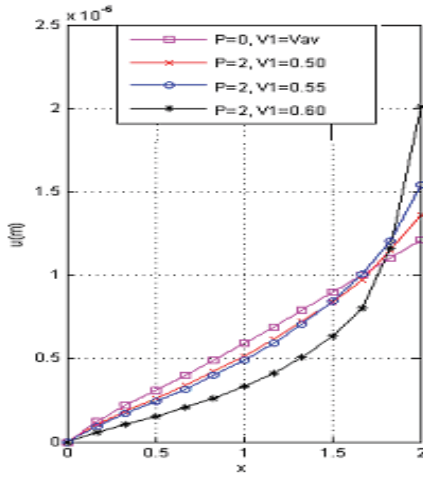


Figure 17: u-displacement result comparison for tension cases with P=0 and P=2

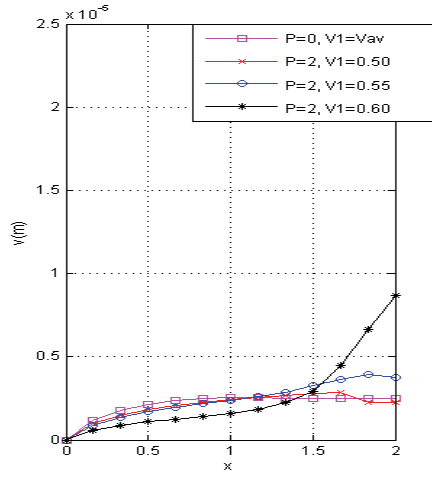


Figure 18: v-displacement result comparison for tension cases with P=0 and P=2

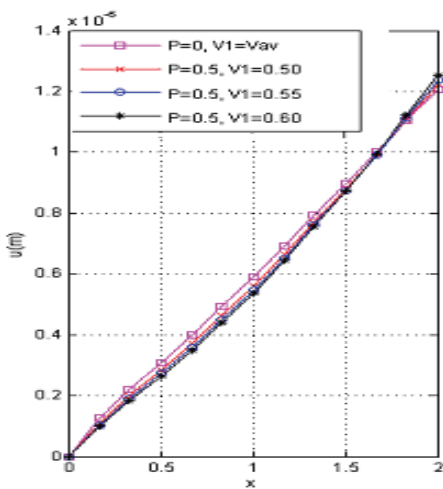


Figure 19: u-displacement result comparison for tension cases with P=0 and P=0.5

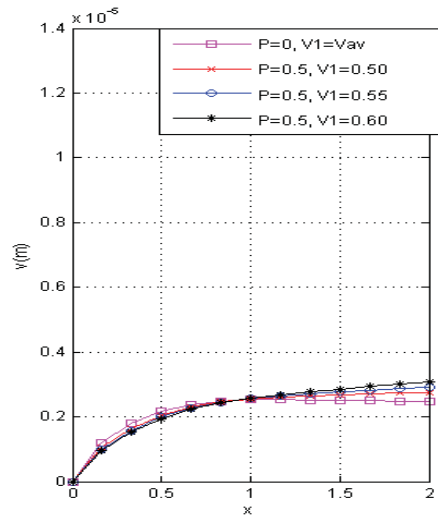


Figure 20: v-displacement result comparison for tension cases with P=0 and P=0.5

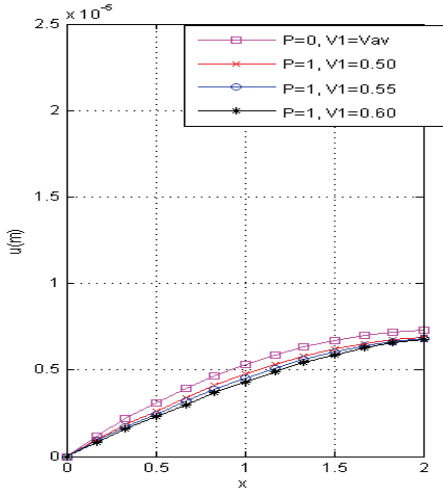


Figure 21: u-displacement result comparison for in-plane bending cases with P=0 and P=1

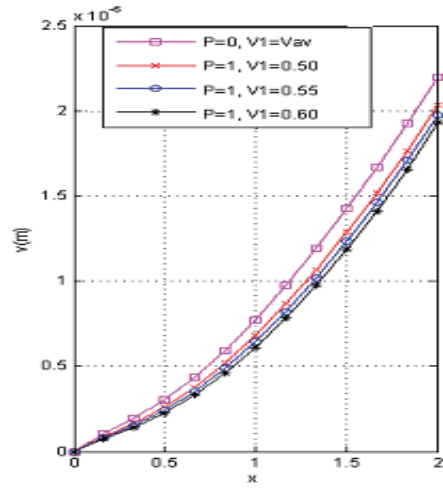


Figure 22: v-displacement result comparison for in-plane bending cases with P=0 and P=1

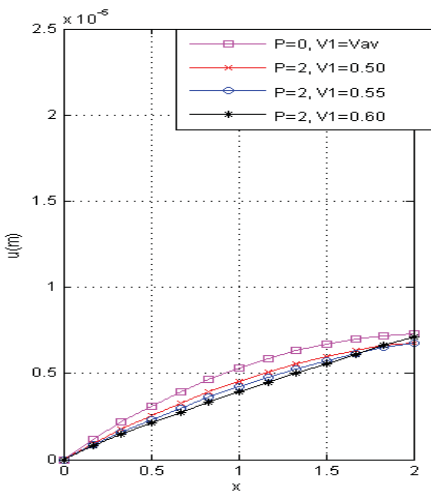


Figure 23: u-displacement result comparison for in-plane bending cases with P=0 and P=2

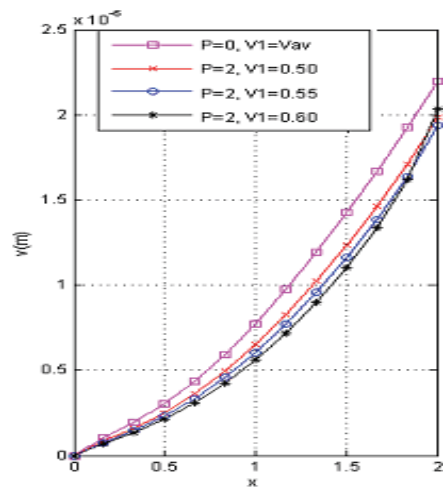


Figure 24: v-displacement result comparison for in-plane bending cases with P=0 and P=2

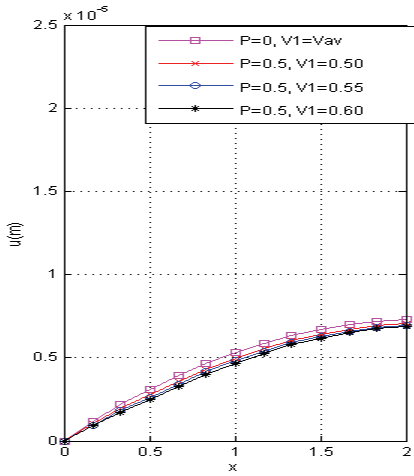


Figure 25: u-displacement result comparison for in-plane bending cases with P=0 and P=0.5

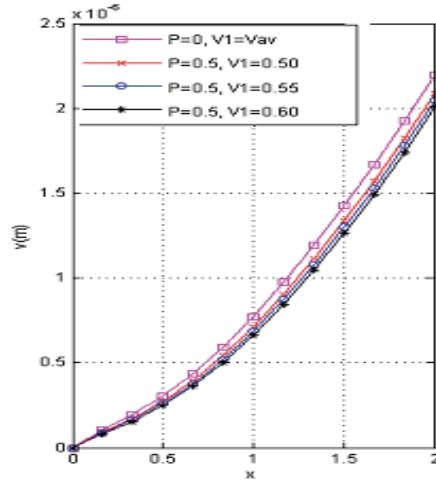


Figure 26: v-displacement result comparison for in-plane bending cases with P=0 and P=0.5

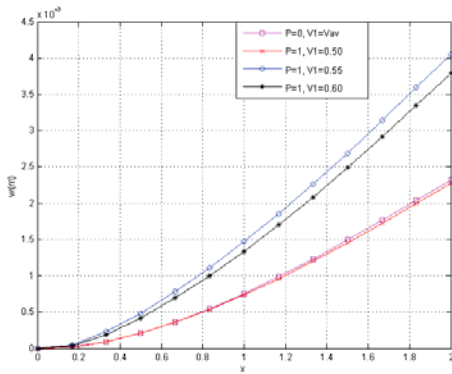


Figure 27: w-displacement result comparison for out-of-plane bending cases with P=0 and P=1

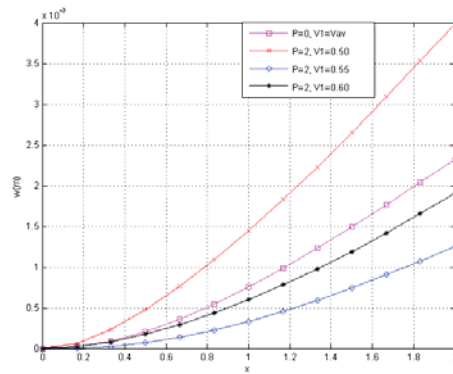


Figure 28: w-displacement result comparison for out-of-plane bending cases with P=0 and P=2

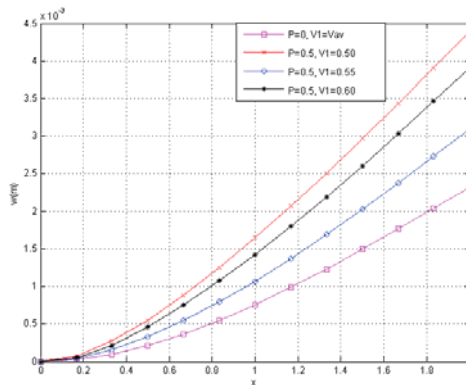


Figure 29: w -displacement result comparison for out-of-plane bending cases with $P=0$ and $P=0.5$

cal limitations of materials or structural properties required for satisfactory performance are not exceeded. This optimisation technique involves changing the fibre distribution parameters and running the three FE codes for the given fibre distribution, checking to see if all constraints have been satisfied. The constraint that has been considered is the displacement constraints. The flow chart below is a good description of this optimisation technique concept.

5.1 Fibre Distribution Effect on Progressive Damage Analysis Result

In this section, progressive damage analysis was carried on a cantilever plate with ten different fibre ratio distribution cases, subjected to tension loading, in-plane and out-of-plane bending. The results obtained are presented below.

Tension Case

Figure 15 and Figure 16 show the comparison of the displacement results for the tension cases with $P=0$ and $P=1$. In this tension case, the parameter that is of major interest is the u -displacement. Minimisation of u -displacement is usually the desired effect for design purposes. Hence Figure 15 shows that the traditional composite case (i.e. $P=0$ and $V1=Vav$) satisfied the minimum u -displacement constraint with a u -displacement of 0.0121mm at edge $x=2$.

Figure 17 and Figure 18 show the comparison of the displacement results for the tension cases with $P=0$ and $P=2$. And it shows that the traditional composite case (i.e. $P=0$ and $V1=Vav$) satisfied the minimum u -displacement constraint with a u -displacement of 0.0121mm at edge $x=2$.

Figure 19 and Figure 20 show the comparison of the displacement results for the

tension cases with $P=0$ and $P=0.5$. And it shows that all four curves overlay on top of each other with negligible result discrepancies. Hence all four fibre distribution cases satisfied the minimum u-displacement constraint with a u-displacement of 0.0121mm at edge $x=2$.

In summary, the above results showed that all the ten fibre ratio distribution cases had no significant effect on the tension case because all ten cases gave identical u-displacement results with negligible discrepancies.

In-plane Bending Case

Figure 21 and Figure 22 show the comparison of the displacement results for the in-plane bending case with $P=0$ and $P=1$. In this in-plane bending case, the parameter that is of major interest is the v-displacement. Minimisation of v-displacement is usually the desired effect required for design purposes. Hence Figure 21 shows that the case with $P=1$ and $V1=0.6$ satisfied the minimum v-displacement constraint with a v-displacement of 0.019mm at edge $x=2$.

Figure 23 and Figure 24 show the comparison of the displacement results for the in-plane bending case with $P=0$ and $P=2$. And it shows that the curves of the cases with $P=2$ overlay on top of each other and their v-displacements are lower in comparison to the traditional composite case (i.e. $P=0$ and $V1=V_{av}$). Hence all the three cases with $P=2$ satisfied the minimum v-displacement constraint with a v-displacement of 0.019mm at edge $x=2$.

Figure 25 and Figure 26 show the comparison of the displacement results for the in-plane bending case with $P=0$ and $P=0.5$. And it shows that the case with $P=0.5$ and $V1=0.6$ satisfied the minimum v-displacement constraint with a v-displacement of 0.02mm at edge $x=2$.

In summary, the above results showed that the in-plane bending case with $P=1&2$ and $V1=0.6$ gave the minimum v-displacement at edge $x=2$ in all ten fibre ratio distribution cases. Hence this fibre ratio distribution case is the best case that satisfied the minimum v-displacement constraint.

Out-of-plane Bending Case

Figure 27 shows the comparison of the displacement results for the out-of-plane bending case with $P=0$ and $P=1$. In this out-of-plane bending case, the parameter that is of major interest is the w-displacement. Minimisation of w-displacement is usually the desired effect required for design purposes. Hence Figure 27 shows that the case with $P=1$ and $V1=0.5$ satisfied the minimum w-displacement constraint with a w-displacement of 2.25mm at edge $x=2$.

Figure 28 shows the comparison of the displacement results for the out-of-plane bending case with $P=0$ and $P=2$. And it shows that the case with $P=2$ and $V1=0.55$ satisfied the minimum w-displacement constraint with a w-displacement of 1.25mm

at edge $x=2$.

Figure 29 shows the comparison of the displacement results for the out-of-plane bending case with $P=0$ and $P=0.5$. And it shows that the traditional composite case (i.e. $P=0$ and $V1=V_{av}$) satisfied the minimum w -displacement constraint with a w -displacement of 2.3mm at edge $x=2$.

In summary, the above results showed that the out-of-plane bending case with $P=2$ and $V1=0.55$ gave the minimum w -displacement at edge $x=2$ in all ten fibre ratio distribution cases. Hence this case is the best case that satisfied the minimum w -displacement constraint.

5.2 Optimum Design

In this paper, the optimum design criterion employed, is one that nearly satisfies the minimum deflection design criteria. Hence, using the definition of design criterion above, the results in the previous sections were tabulated as shown below and the optimum design was determined from the table.

Table 2: Optimum design

P	V1	Tension (u_{fgm}/u_{comp})	In-plane Bending (v_{fgm}/v_{comp})	Out-of-plane Bending (w_{fgm}/w_{comp})
0.5	0.5	1.03	0.94	1.95
0.5	0.55	1.03	0.91	1.33
0.5	0.6	1.03	0.88	1.73
1	0.5	1.03	0.93	0.98
1	0.55	1.08	0.89	1.85
1	0.6	1.17	0.84	1.72
2	0.5	1.08	0.89	1.81
2	0.55	1.25	0.84	0.59
2	0.6	1.66	0.93	0.89

The optimum fibre distribution result for each load cases have been highlighted in the above table. Since the fibre distribution case with $P=2$ and $V1=0.55$ has the most common optimum fibre distribution results, then this fibre distribution case can be said to give the overall optimum design for most load cases. Although this optimum fibre distribution case had adverse results of 125% u -deflection in tension and 92% buckling load relative to the traditional composite case, prioritisation of the constraints need to be undertaken in determining whether these adverse results are good enough trade-offs.

6 Conclusion

In this paper, two new Mindlin-type elements have been formulated and used in performing a finite strain analysis and progressive damage analysis of a functionally graded composite structure. It was shown in the validation exercise that the Smooth Mindlin-type element gave a more accurate result for the out-of-plane bending case because the Average Mindlin-type element requires finer mesh for its result to converge to the result of Smooth Mindlin-type element. After the validation exercise, the Smooth Mindlin-type element was then employed for the design optimisation of the functionally graded composite structure. A methodical approach was used in demonstrating the design optimisation process and an optimum fibre distribution was obtained for the load cases considered. Also this paper achieved its objective by presenting a detailed explanation of the functional graded technology from theoretical concept through to optimum design application. Future work recommendation would be to extend this work to cover non-linear dynamics and thermo-elasticity.

References

- Attia, O.; El-Zafrany, A.** (1999): A high order shear element for non-linear vibration analysis of composite layered plates and shells. *Int. J. Mech. Sci.*; 41: 461-86.
- Chen, X. L.; Liew, K. M.** (2004): Buckling of rectangular functionally graded material plates subjected to nonlinearly distributed in-plane edge loads. *Smart Materials and Structures*, 13, pp.1430-1437.
- Ching, H. K.; Chen, J. K.** (2006): Thermomechanical analysis of functionally graded composites under laser heating by the MLPG method. *CMES: Computer Modeling in Engineering & Sciences*, vol.13, no.3, pp.199-217.
- Criado, R.; Ortiz, J. E.; Mantic, V.; Gray, L. J.; Paris F.** (2007): Boundary element analysis of three-dimensional exponentially graded isotropic elastic solids. *CMES: Computer Modeling in Engineering & Sciences*, vol.22, no.2, pp.151-164.
- Crisfield, M.; Mi, Y.; Davies, G. A. O.; Hellweg, H. B.** (1997): Finite element methods and the progressive failure – modelling of composites structures. *Computational plasticity: fundamentals and applications*.
- Daniel, M. I.; Ishai, O.** (1994): *Engineering mechanics of composite materials*. Oxford University Press.
- Liu, K. Y.; Long, S. Y.; Li, G. Y.** (2008): A meshless local Petrov-Galerkin method for the analysis of cracks in the isotropic functionally graded material. *CMC: Computers, Materials, & Continua*, vol.7, no.1, pp.43-57.

Padhi, G. S.; Sheno, R. A.; Moy, S. S. J.; Hawkins, G. L. (1998): Progressive failure and ultimate collapse of laminated composite plates in bending. *Composite structures*, Vol. 40 No.3-4, pp. 277-291.

Prusty, B G.; Ray, C.; Satsangi, S. K. (2001): First ply failure analysis of stiffened panels – a finite element approach. *Composite structures* 51, 73-81.

Razzaq, R. J.; El-Zafrany, A. (2005) Nonlinear stress analysis of composite plates and shells using a mesh reduction method. *Engineering Analysis with Boundary Elements*. 29, 1115-1123.

Reddy, J. N. (2000): Analysis of functionally graded plates. *International Journal of Numerical Methods in Engineering*; 47: 663-684

Sladek, J.; Sladek, V.; Solec, P.; Wen, P. H. (2008): Thermal bending of Reissner-Mindlin plates by the MLPG. *CMES: Computer Modeling in Engineering & Sciences*, vol.28, no.1, pp.57-76.

Sladek, J.; Sladek, V.; Solec, P.; Wen, P. H.; Atluri, S. N. (2008): Thermal analysis of Reissner-Mindlin shallow shells with FGM properties by the MLPG. *CMES: Computer Modeling in Engineering & Sciences*, vol.30, no.2, pp.77-97.

Sleight, D. W. (1999): Progressive failure analysis methodology for laminated composite structures, NASA/TP-1999-209107

Tolson, S.; Zabar, N. (1991): Finite element analysis of progressive failure in laminated composite plates. *Composite structures* Vol. 38, No. 3, pp. 361-376.

Wen, P. H.; Aliabadi, M. H.; Liu, Y. W. (2008): Meshless method for crack analysis in functionally graded materials with enriched radial base functions. *CMES: Computer Modeling in Engineering & Sciences*, vol.30, no.3, pp.133-147.

